

Article

Development and Characterization of Chitosan-Based Spray-Dried Solid Dispersions of Apigenin: 3D Printed Shell-Pill for Improved Efficacy of Model Flavonoid

Amer Alali ¹, Mohammed Muqtader Ahmed ^{1,*}, Farhat Fatima ¹, Md. Khalid Answer ¹, Mutasim¹, Jamel Patel ³

¹. Department of Pharmaceutics, College of Pharmacy, Prince Sattam Bin Abdulaziz University, P.O. Box 173, Al-Kharj 11942, Saudi Arabia

². Kurtoom University, Sudan

³. Riyadh Elm University, Riyadh, Saudi Arabia

* Correspondence: mo.ahmed@psau.edu.sa

Abstract: This study aimed to develop chitosan-based apigenin spray dried solid dispersion using 1:1,1:1.5,1:2 w/w ratios. The results of process yield and drug assay were found to be (87.5%, 94.2%, and 95.86%), (95.2 ±1.34%), (99.5 ±0.85%), and (97.6 ±2.42%), respectively, for AC1, AC2, and AC3. Flow properties indicate the free flow of powders. FTIR revealed compatibility among chitosan and apigenin, and DSC and XRD showed prepared solid dispersion was on a molecular level and available in amorphous. In contrast, SEM images reflect irregular block and near-spherical shape elongated particles in the selected AC2. The antimicrobial examination reflects that AC2 was more effective against Gram-positive, negative, and fungal strains. AC2 SDDSs has more anti-oxidant property compared to pure flavonoid (AGN). Anti-proliferative activity against A549 lung cancer cell lines showed better anti-cancer activity by AC2 SDDSs. The selected AC2 SDDS filled in a 3D shell pill and further characterized for 3D shell pill for dissolution profiles and stability studies. The product has sustained release and similar release profiles after three months of storage. The findings suggest that the AC2 SDDSs may be a promising candidate for further development as a 3D printed drug delivery system for treating multiple disease conditions using model flavonoid- apigenin.

Keywords: Chitosan; Apigenin; Spray Dried Solid Dispersion; FTIR; DSC; XRD; SEM; 3D; Shell Pill

1. Introduction

Chitosan (CTN) is a natural biocompatible and biodegradable derived from chitin; it has many desirable properties, including being non-toxic, water-soluble, and mucoadhesive properties, which allow it to adhere to mucosal surfaces and improve drug delivery [1],[2]. CTN has a variety of potential applications in industries such as pharmaceuticals, biotechnology, agriculture, and food [3]. CTN can be extracted from the shells of shrimp crabs and lobsters by deproteinization, demineralization, and deacetylation, which involves removing the acetyl groups from the chitin molecule, resulting in a positively charged polymer [4]. It can also be obtained from other than seafood waste, such as fungi, insects, and red or brown algae; extraction can be done from the mycelium of fungi such as *Aspergillus niger* or the exoskeletons of insects such as beetles or cockroaches [5]. Commercially, CTN is available as purified and processed into various forms, such as powder and flakes. CTN has a high molecular weight, which can vary depending on the source of the chitin and the degree of deacetylation. The molecular weight of chitosan can affect its solubility, viscosity, and other properties. The solubility of CTN suggests; insoluble in water at neutral pH but addition of acetic acid improves the solubility due to the of amino groups in its structure [4] (fig-1).

CTN has been used as a drug delivery system due to its unique properties, such as mucoadhesion, permeation enhancement, and controlled drug release. It is widely utilized in the development of nanoparticles, microparticles, hydrogels, and films. CTN is reported to be applied for the delivery of therapeutic moieties, such as anti-cancer agents, antibiotics, and anti-inflammatory agents [6]. Microencapsulation prepared by CTN was exploited to deliver proteins, peptides, and vaccines [7]. Muqtader et al. reported chitosan-based gels for wound healing activity [8]. Studies also reflect the transdermal and buccal films loaded with timolol and nicotine [9]. Cation of the CTN accelerates the adherence of the drug delivery systems (DDSs) on the mucosal surface of the body, such as ocular, nasal, gastrointestinal, respiratory, rectal and vaginal mucosa. This can enhance drug absorption and bioavailability and increase the drug's residence time at the site of action [10]. CTN can also improve drug permeation blood-brain barrier (BBB) due to its ability to open tight junctions between cells [11]. Brigatinib loaded in PLGA nanoparticles coated with CTN was explored for treating non-small cell lung cancer [12]. CTN-coated Buspirone-loaded nanostructured lipid carriers for intranasal delivery used for a nose to brain delivery [13]. *In Vivo*, Pharmacokinetic Studies of CTN-coated PLGA-based NPs showed enhanced bioavailability of Olaparib [14].

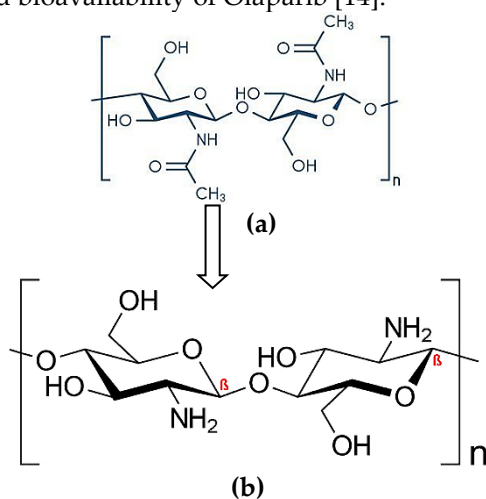


Fig. 1. Framework of (a) Chitin and (b) Chitosan.

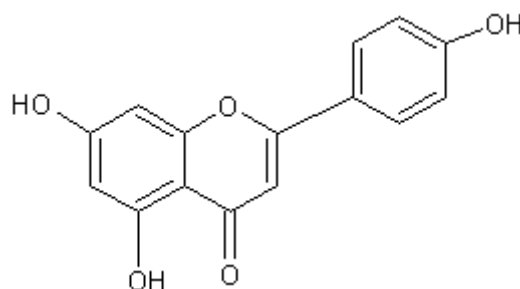


Figure 2. Chemical structure of Apigenin.

Apigenin (AGN) is a flavonoid found in plants; parsley, chamomile, and celery. AGN has multiple health benefits, some reported herein [15]. AGN has the sequestering property, which arrests the free radicals causing oxidative stress, thereby protecting the cells from damage due to cancer, aging, and inflammation. AGN has been shown to have anti-inflammatory properties by inhibiting the activity of cyclooxygenases (COX) and lipoxygenases (LOX), enzymes involved in the production of prostaglandins and leukotrienes inflammatory molecules and also inhibit the activation of nuclear factor-kappa B (NF- κ B), thereby reducing chronic, necrotic and immune regulated inflammation. It's a body's response to injury or infection, but chronic inflammation has been linked to heart disease,

diabetes, and cancer conditions [16], [17]. AGN acts as an anti-cancer agent by regulating the signaling pathways involved in cell cycle progression, angiogenesis, and metastasis, thereby inhibiting the growth of cancer cells, including breast, prostate, colon, lung cancer cells, and reducing the risk of certain types of cancer. AGN-induced apoptosis process may help to prevent the spread of cancer [18]. AGN has been shown to have anxiolytic properties by acting on the gamma-aminobutyric acid (GABA) in the brain, thus regulating anxiety. It also modulates serotonin and dopamine neurotransmitter, which are responsible for anxiolytic effects and are used in Alzheimer's and Parkinson's disease [19]. The antimicrobial activity of AGN is very significant; it inhibits the growth of certain bacteria, viruses, and fungi by disrupting the cell membrane of microorganisms, which can lead to cell death.

Moreover, AGN has also been found to interfere with the enzyme activity involved in bacterial metabolism and DNA replication, which can further contribute to its antimicrobial effects. This makes it a potentially valuable natural remedy for various infections [20]. As the AGN arrests the reactive oxygen species (ROS) in the body, which can help protect against damage to blood vessels and reduce the risk of atherosclerosis [21]. Additionally, it prevents blood clots and improves endothelial function, thereby helping to reduce blood pressure, improve blood lipid profiles, and reduce the risk of heart disease [22],[23]. AGN reflects anti-diabetic properties by improving insulin sensitivity and glucose uptake in cells. It inhibits the enzymes involved in carbohydrate metabolism, thereby supporting the anti-diabetic effects. This makes it a potentially useful natural remedy for diabetes and related complications [24].

AGN is a yellow crystalline powder with a bitter taste, widely used as a drug carrier and therapeutic active both. It's sparingly soluble in water but soluble in organic solvents such as dichloromethane, chloroform, ethanol, methanol, and dimethyl sulfoxide (DMSO). The pKa value of AGN is 7.98, maximum absorption of UV-Vis light is at 272 nm [25], [26]. AGN has been investigated for its potential use in drug delivery systems. Comparative apoptosis study of doxorubicin alone and AGN as a drug carrier enclosed with doxorubicin showed better anti-cancer effects of AGN – doxorubicin than doxorubicin alone [27]. Another study showed that AGN binds to mucous membranes in the body and improves drug absorption [28]. Additionally, AGN nanoparticles of curcumin showed improved solubility and bioavailability of curcumin, leading to enhanced therapeutic effects [29].

Solid dispersions (SDs) have shown promising results in improving the bioavailability of poorly soluble drugs and are widely used in the pharmaceutical industry. SDs are the formulation matrix of molecularly dispersed hydrophilic or amphiphilic polymers, which improves the solubility, dissolution rate, and bioavailability of poorly soluble drugs. The drug can exist in various forms, including crystalline, amorphous, or a combination of both. An amorphous form of the drug relatively has a better dissolution rate and therapeutic effects with reduced doses [30], [31], [32]. Technologies employed in preparing SDs are solvent evaporation, freeze-drying, hot-melt extrusion, and spray drying [33]. Spray drying technology is a commonly used technology for preparing SDs in the pharmaceutical industry and lab setups [34]. In this process, a solution is prepared by dissolving the drug or active moieties (AGN) and a polymer or naturally derived product (CTN), which is then atomized into an air chamber supplied with hot air. The resulting powder consists of drug-polymer particles in a solid state called spray dried solid dispersions (SDSDs) [35]. MM Ahmed *et al.* reported the improved dissolution and aphrodisiac activity of sildenafil and tadalafil SDSDs using glycyrrhizin [36], [37], [31]. Spray-dried amorphous solid dispersion of diosmin in soluplus was prepared by MK Anwer and reported to show improved hepato-renal protective and anti-oxidant properties [38].

3D printing is a promising technology in the pharmaceutical industries and drug development, especially for personalized medicines[39]. In this technique, tailoring drug dosage is possible to meet the patient's compliance and need. The printable materials used are biocompatible and biodegradable; 3d printed dosage form can be fabricated using a

computer-generated model and printer filled with drug-polymer solutions or supplied with filament to design the pill, printlet with precise and complex geometries that would be impossible to create using traditional manufacturing tools. Recent past, FDA approved 3D printed dosage form for the delivery of an anti-epileptic drug, spritam [40]. PVA filament-based 3D printing refers to a 3D printing process where a PVA (polyvinyl alcohol) filament is used as the printing material. PVA is a synthetic polymer that is soluble in water, and non-toxic material, which makes it an ideal material for creating support structures for 3D-printed pills, printlets, and shells [41].

To the best of authors knowledge investigation of spray dried solid dispersion of apigenin with chitosan not yet been reported. The study aimed to develop and characterize chitosan-based spray-dried solid dispersions (SDSDs) of apigenin. First, we prepared the chitosan-based SDSDs of apigenin by optimizing the process parameters such as the concentration of chitosan, the ratio of apigenin to chitosan, and the spray-drying conditions. Characterization parameters include Fourier-transform infrared spectroscopy (FTIR), differential scanning calorimetry (DSC), X-ray diffraction (XRD), and scanning electron microscopy (SEM). Finally, we also fabricated a 3D printlet using PVA filament filled with AGN-CTN SDSDs and assessed their release behavior and content analysis.

2. Results and Discussion

2.1. Process yield-percentage

The calculated yield of AC1, AC2, and AC3 were found to be 87.5%, 94.2% and 95.86%, respectively. During the unit operations of weighing, mixing, agitations, material adherence to the glassware, and pipping used in the spray-drying operation could be the factors for the loss of yield. The higher experiential yield was found to be for AC3 SDSD.

2.2. Drug assay

The drug assay of three batches revealed that the amount of active pharmaceutical ingredient (AGN) in the SDSDs was within pharmacopoeial limits. The percentage of AGN in AC1, AC2, AC3 were found to be results (95.2 ±1.34%), (99.5 ±0.85%), and (97.6 ±2.42%), respectively. As per the USP monograph, the drug content limit should be between 98.0% to 102.0%, which is a legally acceptable guideline for the quality control of drug products. These results confirmed that only batches AC2 and AC3 are acceptable for further optimizations and characterization studies. However, this test is just one quality control test, but to ensure the overall quality and efficacy of the drug product, more QC tests must be performed [42].

2.3. Flow properties of SDSDs

2.3.1. Carr Index and Hausner Ratio

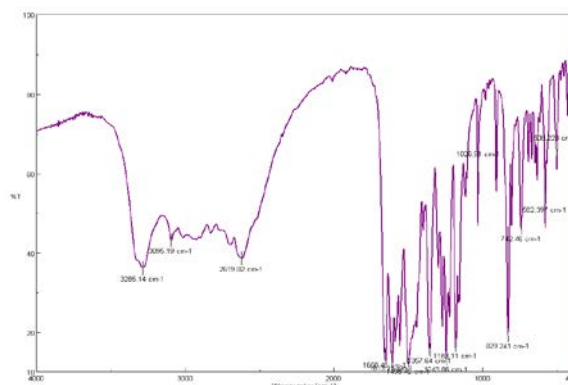
The results of Carr Index AC1, AC2, and AC3 were found to be (13.04%, 15.38%, and 14.28%), with noted Hausner Ratio;1.15, 1.18, 1.16, respectively. All three batches were found to exhibit good/free flow as per these results, which are within the range of the Carr Index (11–15%) and for the Hausner Ratio (1.12–1.18), indicating a free flow of powders.

2.3.2. Angle of repose

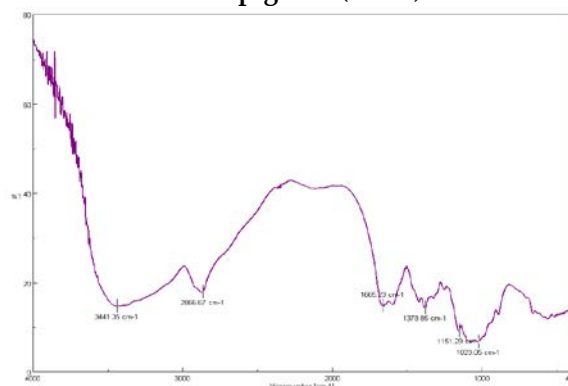
The angle of repose is an indication of the degree of agglomeration or clustering of the particles in the powder. It is related to the interparticle forces and the particle size distribution of the powder. The results of SDSDs were found to be 22.3±0.14°, 20±0.21° and 27±0.11° for AC1, AC2, and AC3, respectively. All SDSDs were found to have good flow characteristics as the values of the angle of repose ranged between 20° to 30° [43]. By measuring the angle of repose of the SDSDs, one can determine whether the prepared product has the desired flow properties and whether the particle size distribution is suitable for the intended application, filling in the 3D printlet.

2.4. FTIR spectroscopy

The FTIR spectrum of apigenin typically shows peaks that represent (3285.14 cm^{-1}) O-H stretching of the phenolic group, (3095.19 and 2619.82 cm^{-1}) C-H stretching of the aliphatic groups, (1668.48 cm^{-1}) C=O stretching of the carbonyl group, (1613.1 cm^{-1}) C=C stretching of the aromatic ring, (1498.42 cm^{-1}) C-H bending of the aromatic ring, (1243.86 - 1183 cm^{-1}) C-O stretching of the carbonyl and ether groups. In the case of the chitosan (CTN) spectrum, the peak at around (3441.35 cm^{-1}) corresponds to the stretching vibration of the O-H and N-H groups in chitosan, indicating the presence of hydrogen bonding (2666.67 cm^{-1}) stretching vibration of the C-H bonds in the chitosan backbone and the acetyl groups, (1665.23 cm^{-1}) stretching vibration of the C=O bond in the acetyl groups, (1378.85 cm^{-1}) stretching vibration of the amide bond (C=O and N-H) in the chitosan backbone and the peak at (1151.29 cm^{-1}) indicating bending vibration of the CH₃ groups in the acetyl groups. Another broad peak at (1023.05 cm^{-1}) corresponds to the stretching vibration of the C-O-C bond in the chitosan backbone. In the FTIR spectrum of a SDS of chitosan apigenin (AC2), bands corresponding to the stretching and bending vibrations of CTN (such as the amide bands at around (1650.77 cm^{-1} and 1465.63 cm^{-1}), as well as bands corresponding to the functional groups present in AGN (such as the aromatic ring vibrations at around 1223.61 cm^{-1} and the carbonyl group at around 1959.57 cm^{-1}). Apart from these there are many individual peaks exhibited in AGN and CTN present in the AC2 without any significant modifications indicating AGN and CTN are compatible with each other and doesn't show any physicochemical interactions and formation of new bond or compound. FTIR spectroscopy is a valuable tool for analyzing chemical compounds and can provide important information on their composition, structure, and interactions.



Pure apigenin (AGN)



Chitosan (CTN)

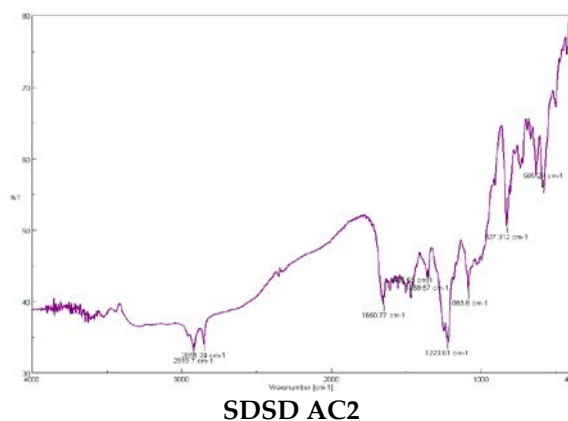
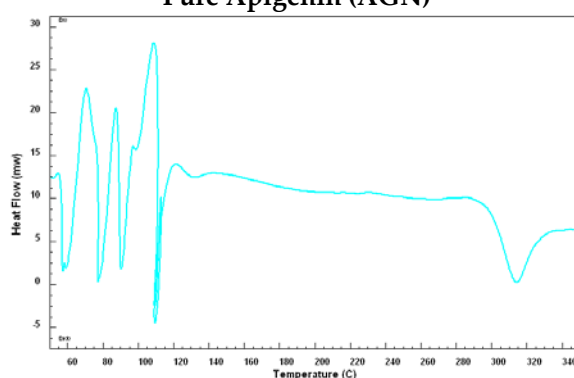
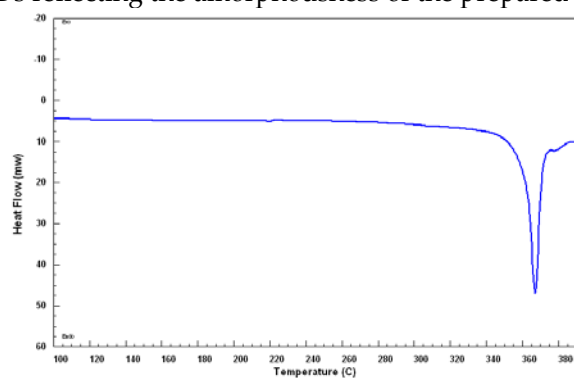
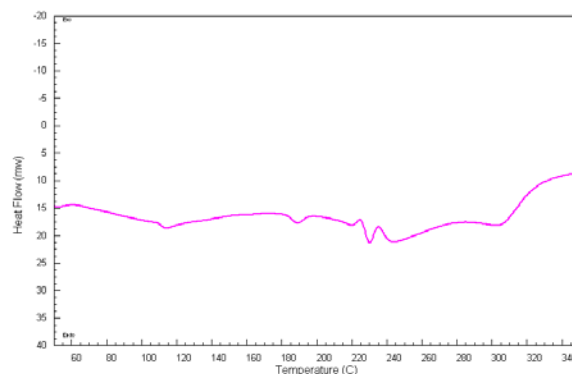


Figure 3. FTIR spectrums of AGN, CTN and AC2.

2.5. Differential scanning calorimetry

The DSC thermogram of AGN typically shows a single endothermic peak at 365°C, the corresponding melting point of the flavonoid compound. Chitosan thermal peak was observed at 110°C due to the melting transition indicated by a sharp endothermic peak, which could shift and corresponds to the deacetylation and the molecular weight of the polymer used in the study. At higher melting temperatures >315°C, CTN begins to decompose. The thermogram of SDSD (AC2) doesn't have any intense exothermic or endothermic peaks indicating AGN was molecularly dispersed within the CTN, this is a desirable property of SDs reflecting the amorphousness of the prepared product [44].



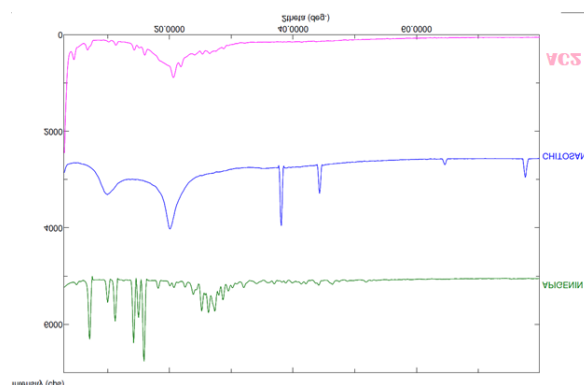


SDSD (AC2)

Figure 4. DSC thermograms of AGN, CTN and SDSD (AC2).

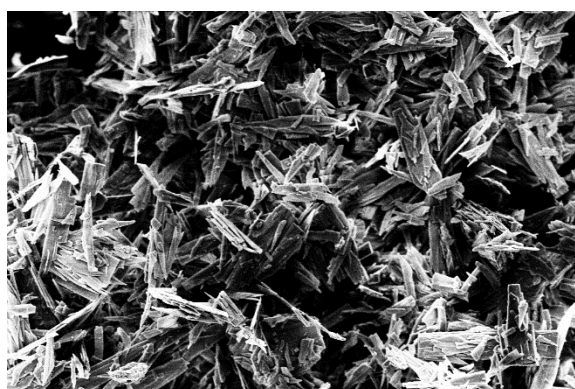
2.6. X-ray crystallography

X-ray diffraction pattern of AGN showed diffraction peaks at 2θ values of 5.8° , 11.4° , 12° , 14° , 16.5° , 18.4° , 22.3° , and 26.4° suggesting crystalline structure with a monoclinic space group form of flavonoid (AGN) used in this study. CTN exhibits broad peaks at around 2θ ; 10° and 20° indicating a mixture of crystalline and amorphous or disordered nature of chitosan. Additional peaks at 38° and 42° is due to the degree of deacetylation and the crystallinity of the material. In the diffractogram of SDSD AC2, the peaks of both chitosan and apigenin are expected to be present, but their intensities were reduced with a shift in positions. Reduction in the intensities of the peak indicates the solid state of the product is available in the non-crystalline form, presence of few peaks designates – typically a few percent of crystalline forms.

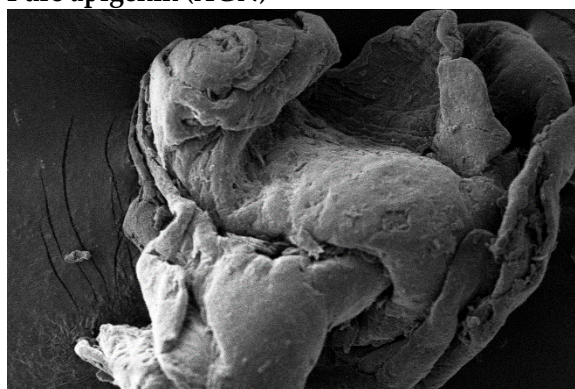
**Figure 5.** X-ray diffraction patterns of AGN, CTN and SDSD (AC2).

2.7. Scanning electron microscopy

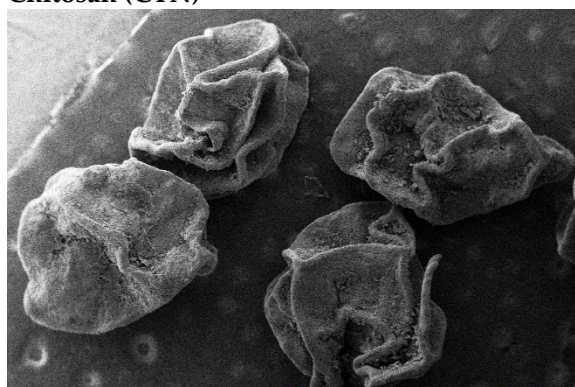
The SEM image of pure apigenin (AGN) reflects irregular block and near-spherical shape elongated particles, which means that the particles have some level of variability in their shape. CTN image showed porousness and rough shape, whereas the SDSD AC2 showed a spherical shape with a shriveled surface and wrinkled or uneven.



Pure apigenin (AGN)



Chitosan (CTN)



SDSD (AC2)

Figure 6. SEM images of AGN, CTN and SDSD (AC2).

2.8. Antimicrobial assay

Prepared SDSD of AGN (AC2) was assessed for antimicrobial test against the different microflora of Gram-positive (*S. Aureus*, *B. subtilis*), Gram-negative (*E. coli*) and fungi (*C. Albicans*) in order to check its effectiveness on a broad spectrum. The zone of inhibition of AC2 compared with the pure AGN to ensure the developed SDSD has more therapeutic potential. The larger the zone of inhibition, the more effective the antimicrobial agent is against the microbe. For *S. Aureus*, both AGN and AC2 showed good activity with a zone of inhibition values of $(17 \pm 1.47$ and 19 ± 1.65 mm), respectively. Similarly, for *B. subtilis*, the two agents demonstrated similar activity with a zone of inhibition of $(18 \pm 1.75$ and 19 ± 1.18 mm), respectively. However, for *E. coli*, both AGN and AC2 demonstrated lower activity with a zone of inhibition of $(13 \pm 1.38$ and 16 ± 1.43 mm), respectively. This suggests these agents may not be as effective against this strain as the others.

On the other hand, for *C. Albicans*, both AGN and AC2 showed good activity with a zone of inhibition of $(20 \pm 1.03$ and 22 ± 1.63 mm), respectively. This indicates that these

agents are highly effective against this fungal strain. The results suggest that AGN and AC2 have varying degrees of antimicrobial activity against different strains of microorganisms, AC2 was more effective against pure AGN. Published reports suggested that AGN exerted an antibacterial and antifungal activity by inducing membrane disturbances, leading to cell shrinkage, leakage, and organism death [44].

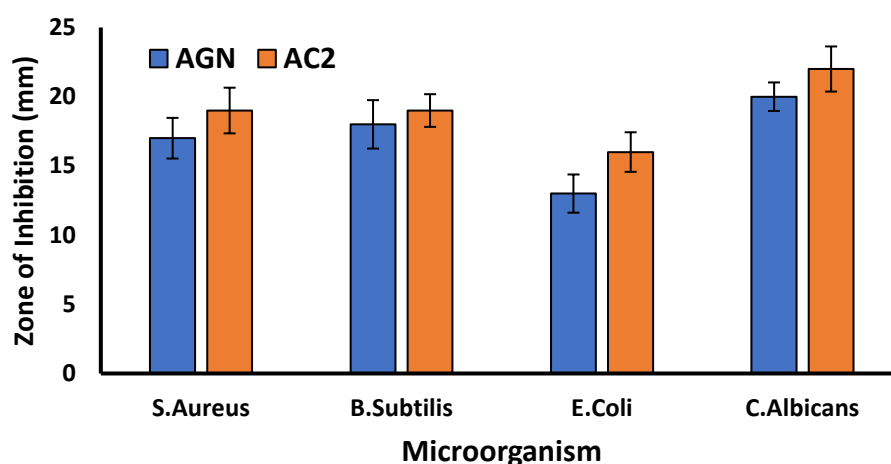


Figure 7. Zone of inhibition (mm) of AGN and SDSD (AC2) against different microbial strains.

2.9. Anti-oxidant study

The anti-oxidant activity was performed for pure flavonoid (AGN) and the AC2 SDSDs, at concentrations 200 - 1000 ppm; the DPPH scavenged activity was found to be in the range of (39.31±2.32 - 61.6±11.32%) for pure AGN and for SDSDs it was noted to be (45.34±1.65 - 92.32±1.76%). APG has a natural anti-oxidant due to its flavonoids property; therefore, pure APG showed the anti-oxidant, but the AC2 SDSDs have increased anti-oxidant effects due to the synergistic effects of AGN and CTN. Chitosan is a natural polymer derived from chitin, which is found in the exoskeletons of crustaceans like shrimp and crabs. Chitosan has been shown to have anti-oxidant properties as well. More studies have reported that the combination of apigenin and chitosan may enhance the anti-oxidant activity of both compounds. Zafar *et.al* investigated the chitosan-based nanoparticles loaded with APG, and results showed enhanced anti-oxidant activity [45]. However, more research is needed to understand the mechanisms underlying this effect fully and to determine the optimal ratios and concentrations of the two compounds for maximizing their anti-oxidant potential. The anti-oxidant mechanism of AGN may involve one or more pathways; Chelating metal ions to stop the formation of reactive oxygen species, increases the expression of superoxide dismutase and suppressing the NADPH oxidase and xanthine oxidase enzymes. APG also scavenges free radicals such as superoxide anion, hydroxyl radical, and peroxynitrite. Thereby donating hydrogen atoms to the free radicals, thereby neutralizing them and preventing oxidative damage to cells. However, chitosan has been reported to show anti-oxidant activity in addition to the aforementioned process, Inhibition of lipid peroxidation, a process in which free radicals attack the unsaturated fatty acids in cell membranes by neutralizing the lipid-derived free radicals. A plot of the percentage of DPPH scavenged against the concentration of the test sample AC2 and AGN is given in fig-8.

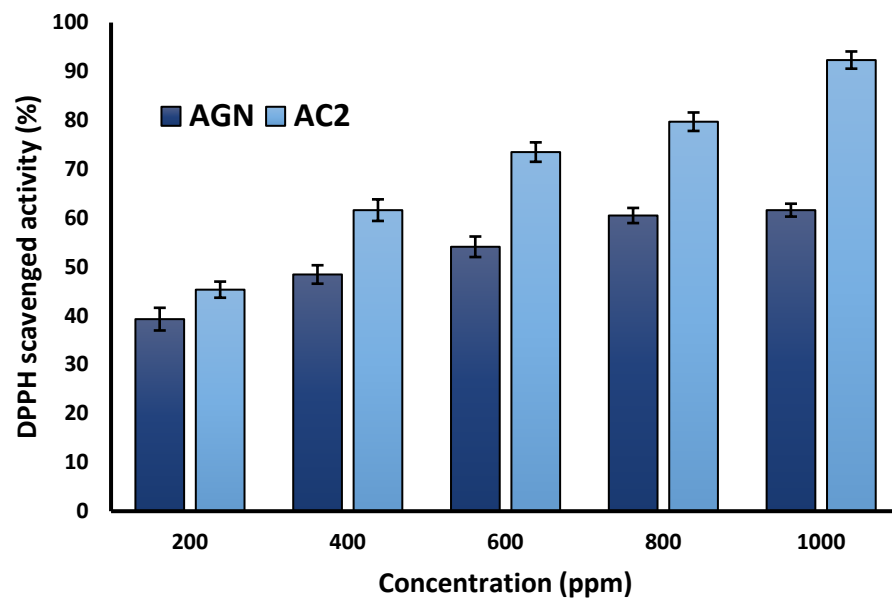


Figure 8. Anti-oxidant effect of AGN and SDS (AC2) at different concentrations.

2.10. Anti-proliferative activity

The percentage of viability of the A549 cells of AC2 SDS was found to be (38.15±1.45%, 24.79± 2.16 %, 16.64 ± 1.34%, 8.15±1.64%) compared to pure AGN (54.46±1.56, 36.51±2.54, 25.64±1.59, 20.84 ±1.35%) at (6.25, 12.5, 25 and 50 µg/ml) concentration. At the highest concentration tested (50 µg/ml), both AGN-Pure and AC2 significantly reduced the viability of the A549 cells compared to the control group (0 µg/ml), indicating AGN was effective against lung cancer. AGN acts as an antiproliferating agent by activating the apoptosis pathway that decreases the PI3K/Akt signaling, triggering cancer cell death and preventing lung tumor [18], [46]. Half maximal inhibitory concentration (IC₅₀) was also calculated, indicating the concentration of a flavonoid (AGN) and product AC2 SDS needed to inhibit the growth of cancer cells by 50%. AC2 has an IC₅₀ value of 3.7707, which was relatively lower than the IC₅₀ value of AGN-Pure, which is 5.3979. In this case, AC2 has an IC₅₀ value of 3.7, which is lower than the IC₅₀ value of AGN-Pure, which is 5.3. This indicates that AC2 is more potent than AGN-Pure in inhibiting the growth or proliferation of cancer cells. These values suggest that AC2 is more potent than AGN-Pure in inhibiting the biological activity or process being studied.

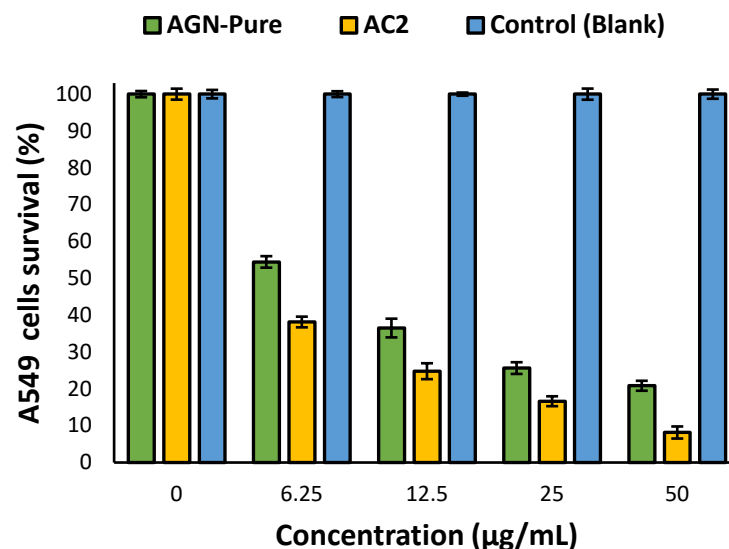


Figure 9. Anti-proliferating effect of AGN and SDS (AC2) against A545 lung cancer cell-lines.

2.11. Fabrication of 3D printed PVA shell – pill

The 3D printed PVA shell pill fabrication is an innovative approach to creating a capsular shell-pill design using pre-fabricated PVA filaments and a 3D printer. This method allows for the creation of complex geometries that would be difficult or impossible to achieve using traditional manufacturing methods.

One of the key advantages of this approach, the fabricated shell could be used to store/fill the SDS of AGN (AC2) with precision and accuracy an equivalent of 50mg AGN, a reported daily dose of flavonoid (AGN). The shell pill was filled with 125mg of AC2. The capsular shell-pill design allows for the sustained release of AGN, which can even be tailored by adjusting the filling amount to meet specific patient needs. This makes it an ideal solution for personalized medicine and drug delivery. Using pre-fabricated PVA filaments also simplifies the manufacturing process, eliminating the need for complex tooling and molds. This reduces production costs and lead times, making it a more efficient and cost-effective solution.

2.12. Dissolution profile and release kinetic

Dissolution profiles of the pure (AGN) and AC2 3D Shell Pill depicted in fig10, the results showed that there was a burst release of AGN from the shell pill after 30min with (22.76±0.74%) compared to pure AGN (7.98±0.77%). Therapeutics, with an initial quick-release followed by a more sustained one, is advantageous for maintaining the optimal blood concentration of the medication in patients [42].

As time progressed, active moieties in both the dissolution baskets continued to release at different rates. By approaching 24h, pure AGN released was (25.47±0.46%), while AC2 3D Shell Pill had released (86.73±2.64%). About 2.40 folds improvement in the drug release was observed from the AC2 3D Shell Pill compared to the pure AGN. Moreover, AGN-CTN inclusion may further improve the efficacy of AGN as CTN enhances the permeability across the GI tract due to its mucoadhesive qualities and capacity to open tight junctions.

The kinetics models proposed for the release mechanism revealed correlation coefficient R^2 indicating; 0.68 (zero-order), 0.91 (First-order), 0.90 (Higuchi-model), and 0.96 (Korsmeyer-Peppas), respectively. All these four models are pictured in the fig-11. Based on the (R^2) Korsmeyer-Peppas was considered to be the best-fitted model for AC2 SDS filled shell-pill.

The Korsmeyer-Peppas is an empirical model to describe drug release from flavonoid-polysaccharides (AGN-CTN) matrices. It can be used to describe various types of release kinetics, including Fickian diffusion, non-Fickian release, and case II transport. Moreover, the model allows for determining the release mechanism by diffusion exponent of n value (0.288). This suggests that the release mechanism is non-Fickian or anomalous diffusion, indicating that factors such as swelling or erosion of the CTN matrix or the presence of channels or pores in the matrix may contribute to the AGN release process.

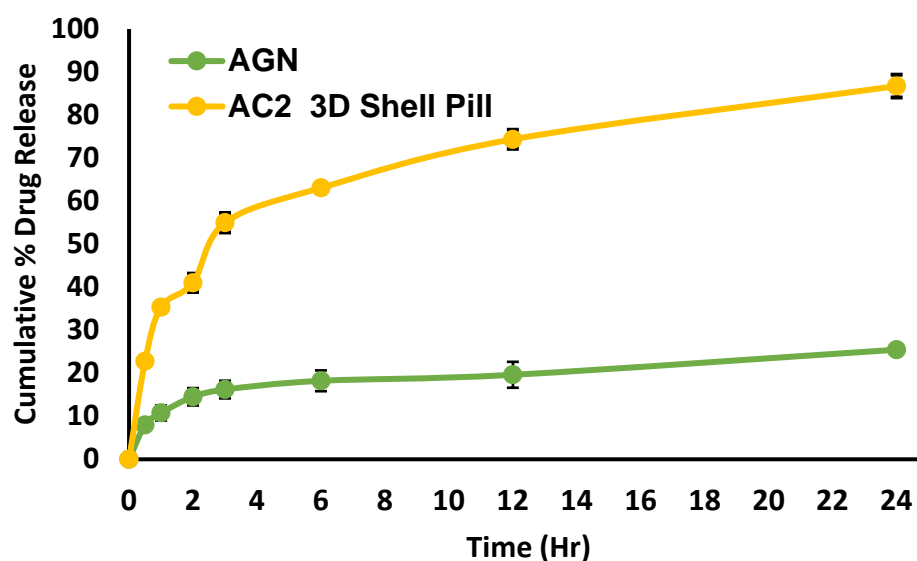


Figure 10. Dissolution profile of AGN and shell-pill filled with AC2 SDS.

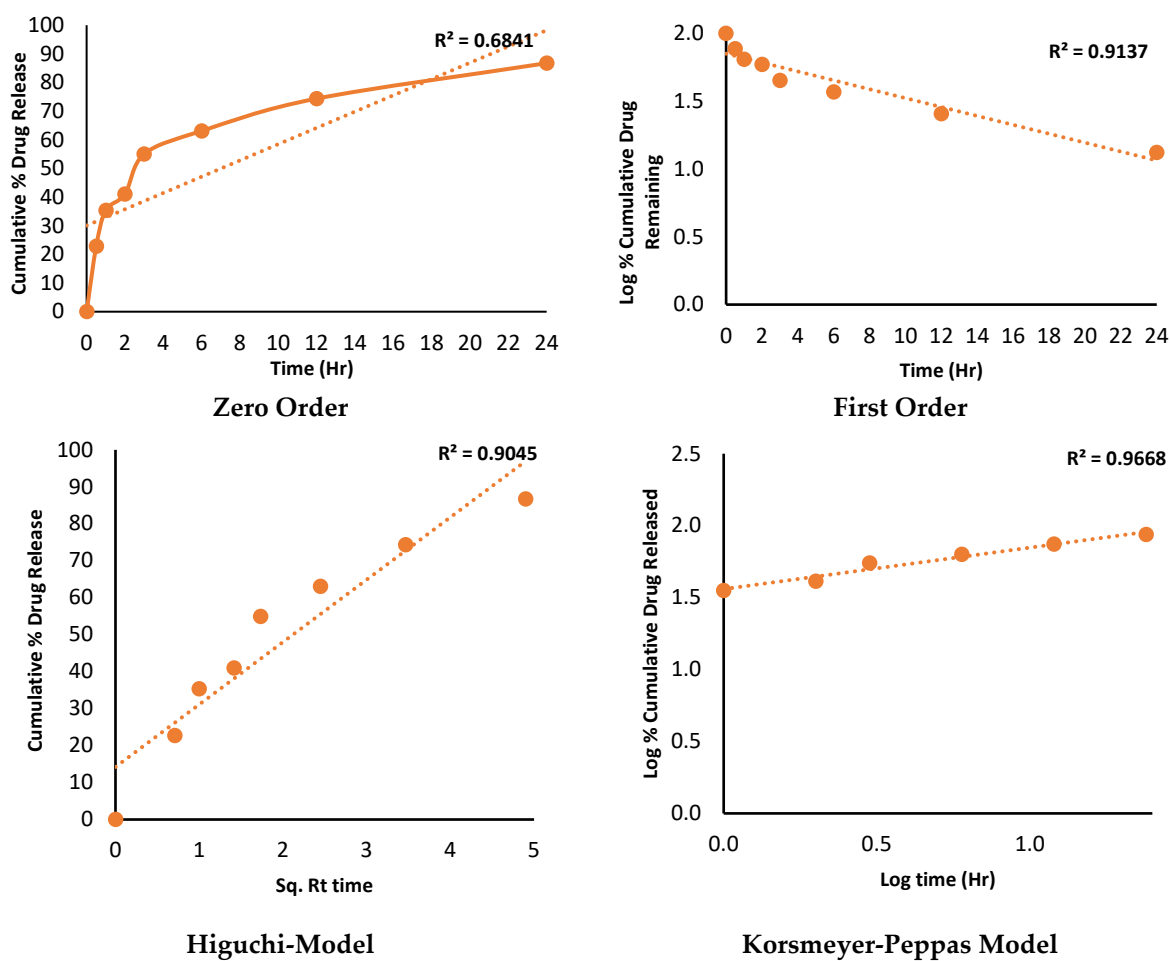


Figure 11. Release kinetics models for shell-pill filled with AC2 SDS.

2.13. Stability studies

The stability study results indicate that the two dissolution profiles of before and after Stability-AC2 SDS filled 3D shell pill have highly similar drug release profiles over

time with a similarity index (f_2) of 51.52. This is supported by a strong positive correlation Pearson coefficient of approximately 0.9949 between the two dissolution profiles. The drug release data shows that both shell pills gradually increase the cumulative % drug release over time.

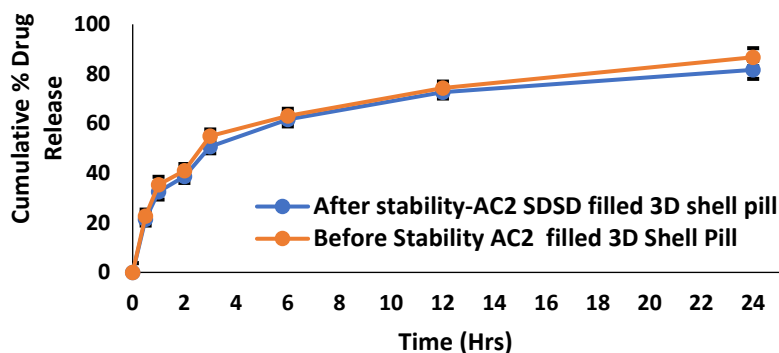


Figure 12. Before and after Dissolution profiles of 3D shell-pill AC2 SDS.

3. Materials and Methods

3.1. Materials

Apigenin was procured from Beijing Mesuchem Technology Co. Pvt. Ltd. (Beijing, China). Chitosan and culture medium used in anti-proliferation studies were obtained from Sigma (St. Louis, MI, USA). Solvents and other chemicals were of analytical grades, purchased from Loba Chemie Laboratory of Reagents and Fine Chemicals.

3.2. Preparation of chitosan-based spray-dried solid dispersions (SDSDs) of apigenin

Apigenin-encumbered SDSDs were prepared using chitosan by spray drying technology. Flavonoid and polysaccharide ratios of 1:1 (AC1), 1:1.5 (AC2), and 1:2 (AC3) w/w (g/g) were selected for the preparations of apigenin-chitosan SDSDs. Chitosan was first dissolved in aqueous acetic acid 1% (v/v); the mixture was then kept on a magnetic stirrer overnight to obtain a homogenous solution. The required amount of AGN dissolved into the ethanol and ultra-sonicated for 2 minutes to complete dissolution. Aqueous (chitosan solution) and organic (AGN solution) were then mixed in a proportion of 60:40. Both solutions were homogenized by a high-speed homogenizer (Wiggins GmbH; Model: D-500, accessories SS20FER20, made in Germany). AGN-CTN dispersion was then pumped into the spray dryer (Buchi Mini Spray Dryer, Model-B-290. Made in Switzerland). The parameters optimized were inlet temperature (80 °C), aspiration (90%), flow rate (15mL/min), in nitrogen environment (28-30 flow rate). The process involved the sprinkling of dispersion through the nozzle (0.5 mm) in a hot air chamber, dried powder formed passed through a cyclone separator and was collected into the jar. Prepared SDSDs were then preserved in the glass vials till further studies [30], [31], [34], [47], [48], [49].

3.3. Process yield-percentage

Spray drying technology involved various unit operations; weighing, mixing, homogenizations and drying. Therefore, the loss of materials (products) need to be calculated in order to endorse the product is economical and process is optimized. Product (SDSDs AC1-3) and the precursors (AGN and CTN) weights were considered to calculate the process yield [30]. The success of manufacturing/product depends on the yield (%).

$$\text{Process yield (\%)} = \frac{\text{weight of SDSD}}{\text{weight of CTN} + \text{weight of AGN}} \times 100$$

3.4. Drug assay

Developed SDDSs containing an equivalent amount of AGN (5mg) were dissolved in aqueous ethanol and mechanically agitated for 24h under a controlled environment of 25 ± 0.5 °C. The aliquots were then pre-filtered through a $0.22\ \mu\text{m}$ syringe filter and analyzed for drug content using ultraviolet spectroscopy at $\lambda_{\text{max}}\ 272\text{nm}$ (Jasco spectrophotometer V-630, Tokyo, Japan). The absorbance of the test was compared with the standard, and concentration (%) was calculated [50].

3.5. Flow properties of SDDSs

3.5.1. Carr Index and Hausner Ratio

Bulk and tapped density were measured by charging the weight amount of SDDSs (AC1-3) in the measuring cylinder noting down the volume it's (bulk volume), followed by tapping it in Pharma Test apparatus (PT-TD200; Hainburg, Germany), to get the tapped volume. Calculate the density (ρ) from (weight/volume) and compute the values in the equations to get the Carr index and Hausner ratio. Both Carr Index and Hausner Ratio are two pre-formulation parameters used to evaluate the flow properties of powders. Carr Index indicates flowability, whereas Hausner Ratio provides compressibility of prepared SDDSs. Low Carr Index and Hausner Ratio are required for better filling of the selected batch into the 3D printlet.

$$\text{Carr index} = \frac{\rho_{\text{tapped}} - \rho_{\text{bulk}}}{\rho_{\text{tapped}}} \times 100$$

$$\text{Hausner ratio} = \frac{\rho_{\text{tapped}}}{\rho_{\text{bulk}}}$$

3.5.2. Angle of repose

The angle of repose is a parameter that can be used to evaluate the flowability and cohesion of prepared SDDSs (AC1-3). The flow ability of the powders can also be determined by the angle of repose in which the powder is allowed to flow through a funnel, it falls on the surface, and height (h) and radius (r) of the sample heap were measured by laser and the result θ is printed. Pharma test automated powder flow analyzer was used (PTG-S4 Hainburg Germany) to measure the angle of repose (θ). The θ is an angle between the surface of the pile and the horizontal plane [37].

$$\theta = \text{Tan}^{-1} h/r$$

3.6. FTIR spectroscopy

A compatibility test was performed using Fourier transform infrared (FTIR) spectroscopy. AGN, CTN, and selected batch SDDSs (AC2) based on the yield and drug content were individually triturated with KBr. The IR dispersion was then compressed to a pellet and kept in the Fourier transform (FT) to generate the spectrums within the fingerprint region of the molecules 4000 to $400\ \text{cm}^{-1}$. The spectrums were interpreted for the possible chemical interactions between the CTN and AGN [51].

3.7. Differential scanning calorimetry

Thermal analysis of samples (CTN, AGN and AC2 SDDSs) was performed by cramping (5mg) of sample in an aluminum hemispherical pan. The test pan was kept beside the reference (empty) pan. The temperature was then raised from 40 to 350 °C at a 20 °C/min heating rate under nitrogen conditions ($40\text{mL}/\text{min}$). Thermograms of all the samples were analyzed and collaged using software and interpreted [47]. The endothermic peak of AGN was then traced to note down m.p of the flavonoid.

3.8. X-ray crystallography

Crystallography study was performed by Ultima IV diffractometer (Rigaku Inc. Tokyo), operated at voltage/current ($40\ \text{kV}/40\ \text{mA}$) using $\text{Cu K}\alpha$ radiation, scanned with a

speed of 0.500 deg/min in the range of 3 to 50Å (2θ). The samples (AGN, CTN, and SDASDs AC2) were analyzed for Bragg's peaks. The solid nature of the materials could be anticipated with the peaks nature intense peaks indicating crystalline nature, whereas broad/short peaks represent amorphousness [52].

3.9. Scanning electron microscopy

Morphological features of the used materials (CTN, APN, CA2 SDASDs) were performed by coating the sample on the glass slide coated with gold for 2min using 20mA current. Under the negative pressure, the sample was bombarded with an electron beam, and scanned coarse and fine imaging adjustment was done to capture the required zone, shape, and size. Operation at 5 kV with a distance of 8-10 mm, images were obtained by scanning and magnification (SEM- Ultraplus, Zeiss, Germany).

3.10. Antimicrobial assay

Gram-positive bacteria (*Staphylococcus aureus*, *Bacillus subtilis*), gram-negative bacillus (*Escherichia coli*, *Klebsiella pneumonia*), and a pathogenic fungal strain (*Candida albicans*) were used in this study. The composition of bacterial culture includes; nutrient broth composed of peptic digest, yeast, and beef extract fungal growth medium containing Sabouraud dextrose. Growth medium after sterilization was poured into Petri plates after solidification, they were inoculated with microbial strains, and the sample well was bored and filled with CA2 suspension. The plates were incubated and examined for the zone of inhibition [53], [54], [55].

3.11. Anti-oxidant activity

Anti-oxidant effects of AGN, SDASDs (AC2), and ascorbic acid was performed using the 2,2'-diphenyl-1-picryl hydrazyl test (DPPH). In this assay, the DPPH radical, a stable free radical with a deep violet color, is used as a model oxidizing agent. Reference standards were prepared by dissolving DPPH in methanol, (0.1mM) concentration was then diluted further to get 1–100 g/mL. Samples under investigation were also made in serial dilution. The test mixture was then prepared by 0.5mL (sample) individually into 2mL 0.1mM DPPD methanol solution (0.5mL). The reaction was allowed between the sample and DPPH for about half-hour in dark conditions at room temperature (25 °C).

When an anti-oxidant (AGN and SDS – AC2) is added to a solution containing DPPH, it can donate an electron or hydrogen atom to the DPPH radical, which reduces its color intensity. This reduction in color intensity can be measured spectrophotometrically and is used as an indication of the anti-oxidant activity of the compound. A higher percentage of DPPH scavenged by the compound indicates a higher anti-oxidant activity [56]. Absorbance (A) of the test sample (Test) and standard (STD) was taken at λ_{max} 517 nm using UV-spectrophotometer (Jasco V 630, made in Japan).

$$\text{Antioxidant effect (\%)} = \frac{A_{517} \text{ STD} - A_{517} \text{ Test}}{A_{517} \text{ Test}} \times 100$$

3.12. Anti-proliferative activity

Apigenin-chitosan spray dried solid dispersion was tested against the A549 lung cancer cell lines using MTT assay. The selected cell line was cultured in a medium composed of Dulbecco's modified Eagle's medium (DMEM) encompassing 10% fetal bovine serum (FBS), and antibiotics (1% penicillin/streptomycin) added to prevent bacterial contamination from both gram-positive and gram-negative bacteria. Glutamine (2mM), and insulin (0.01 mg/ml) were added to support and facilitate the cell growth that required a large amount of proteins and nucleic acids [57], [58].

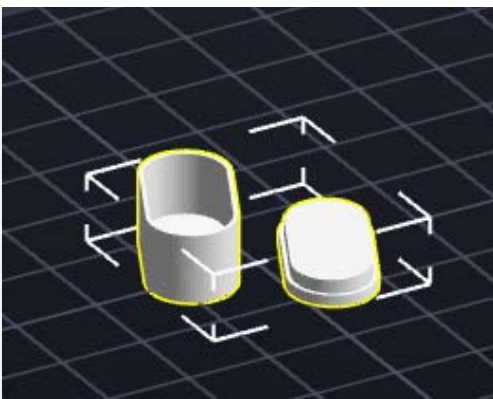
After the 70-80% confluence of cell lines (A549) treated with the AC2 SDSs and pure AGN at different concentrations of (0, 6.25, 12.5, 25, and 50 µg/mL) measure the ability of

cells to convert a colorless substrate into a purple formazan, which has a maximum absorbance at 570nm, using a spectrophotometer. Absorbance is proportional to the number of viable cells. The data obtained are analyzed statistically to determine the significance of the Anti-proliferative activity of apigenin against A549. IC50 was also calculated using Quest Graph™ IC50 calculator.

3.13. Fabrication of 3D printed PVA shell – pill

Pre-Fabricated PVA filaments were used in the fabrication of an FDM-based 3D-Printed shell pill. In order to fill the SDS of AGN (AC2) a capsular shell-pill design was printed using a 3D printer (Easythree X1 Model) with a heating stage [59]. The geometry of the shell -pill was designed by using computer-aided software Autodesk Fusion 360. The 3D capsular shell pill was printed in an oblong shape with a cap and a body. The shell body was filled with AC2, and then the cap was placed over it to seal the shell. The dimension of the capsular shell body was 20mm in length, 10mm in width with 8mm inner depth, and the shell cap was 20mm in length, 10mm in width with 3mm inner layer depth to be get fixed on the body. The shell design was saved as STL (Standard Triangle Language) file, which describes the 3D geometry of the design. This STL file was transferred to a 3D printer software which converts this to a printer-readable G-code (Geometric code for computer numerical control). The G-code for the designed 3D shell was formed by using a 3D printer slicer software Repetier- Host V2.2.4 (with Slic3r Slicer). This G-code comprised all the slicing details for the design and printing parameter settings for the printer. The layer thickness, shell thickness, and initial layer thickness were set to 0.2, 1.2, and 0.3mm, respectively. The infill density was 15% with a rectilinear infill. The printing, travel, and bottom speeds were set to 60, 80, and 20mm/sec, respectively. The low printing speed at the bottom facilitates the adhesion of the initially printed layers to the print bed. PVA filament was fed into the extruder of the 3D printer, wherein the filament gets melted and extruded through the nozzle over a build plate and forms the designed 3D shell pill in a layer-by-layer pattern [60]. The diameter of the loaded PVA filament was 1.75mm, and the extruder nozzle size was 0.4mm. The nozzle temperature was set to 200 0C, and the bed temperature to 60 0C. After printing, the capsular shell body and cap were removed from the printer bed, separated from raft support, filled with AC2, and subjected to further characterization. The printing was carried out without retraction [61].

Table 1. PVA filament based Shell-pill design parameters.

STL file	Slicing parameters		Printing parameters	
 <p>Capsular shell-pill body and cap</p>	Layer thickness	0.2mm	Printing temperature	200 0C
	Shell thickness	1.2 mm	Bed temperature	60 0C
	Initial layer thickness	0.3 mm	Printing speed	60mm/sec
	Infill density	15%	Travel speed	80mm/sec
	Adhesion	Raft	Bottom speed	20mm/sec

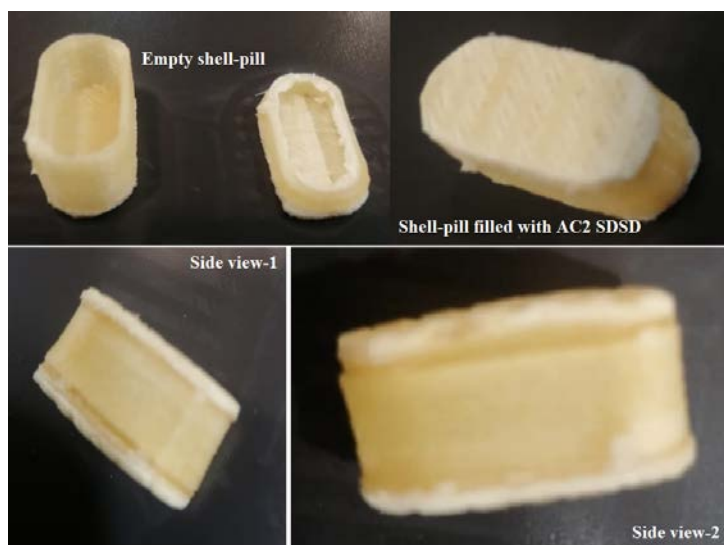


Figure 10. PVA filament based Shell-pill filled with AC2 SDS.

3.14. Dissolution profile and release kinetic

Apigenin–chitosan SDS (AC2) with an equivalent weight of 50 mg of AGN filled in 3D printed shell-pill was placed into the basket (USP- II), filled with medium dissolution 900mL of gastric fluid pH (3) phosphate buffer. Another flask was added pure-AGN (50mg) filled in PVA shell pill. Both flasks were immersed into the water jacket maintained at 37 ± 0.5 °C (Erweka- disso). At predetermined intervals, aliquots of 1mL were withdrawn from each flask and replenished with the fresh medium. Samples were analyzed for the AGN released percentage; the data was then filtered to the release kinetics models to calculate the mechanism of release. The drug quantification was done by using UV spectroscopy at λ_{max} 272nm. Release data computed into the mathematical equations of zero order, first order, Higuchi model and Korsmeyer - Peppas model [62],[63].

3.15. Stability studies

AGN filled PVA shell- pill was exposed to 40 ± 0.5 °C, relative humidity 75%, the pill was kept for 90 days and release study was performed as discussed in the above section. The dissolution profiles of before and after stability test was compared and release data was added into the similarity index (f_2). The f_2 stands for similarity index, n is for dissolution time, R_t and T_t are reference and test dissolution at time t [60]. As per SUPAC if the difference between the release data is ≤ 50 . Then the products said to be similar in drug release, and the environment does not have significant impact on the fabricated pill during storage conditions.

$$f_2 = 50 \times \log\left\{ \left[1 + \frac{1}{n} \sum_{t=1}^n (R_t - T_t)^2 \right]^{-0.5} \times 100 \right\}$$

Similarity metric such as the Pearson correlation coefficient was also calculated for both release profiles AC2 3D shell pill.

3.16. Statistics and software

Microsoft Excel 2016 was used in the release rate and similarity index calculations. The software used for the design of 3D pill was Fusion 360. Analysis was performed using ANOVA (Analysis of variance) if results showed $p < 0.05$ considered significant. All the parameters were performed, and results were taken in $n=3$.

4. Conclusions

This study concludes that the chitosan-based spray-dried solid dispersions of apigenin have demonstrated enhanced drug release, improved antimicrobial activity, anti-oxidant properties, and anti-cancer effects in A549 lung cancer cell lines. Apigenin inclusion in chitosan was developed by spray drying using three ratios (1:1, 1:1.5 and 1:2), characterization of SDSDs were performed for flow properties, and physicochemical and pharmacological evaluations. The selected SDSD (AC2) was further developed in a 3D-printed shell pill, a suitable formulation, and a dosage unit. AC2 SDSD filled 3D shell pill could be a potential dosage unit against A549 lung cancer; this may allow for personalized drug dosage and adjustment of the dose to better fit the patient's needs. Overall, this study suggests that the apigenin chitosan solid dispersion 3D printed pill could be a potential therapeutic with multiple beneficial properties. However, further research and testing may be necessary to fully understand this solid dispersion's potential benefits and limitations for various applications and to evaluate their efficacy and safety *in vivo*.

Author Contributions: “Conceptualization, M.M. and Y.Y.; M.M, M.K.; software, J.P.; validation, A.A. and F.F.; formal analysis, F.F.; investigation, M.M.; resources, A.A.; data curation, A.A.; writing—original draft preparation, M.M.; writing—review and editing, A.A.; visualization, F.F.; supervision, A.A. All authors have read and agreed to the published version of the manuscript.

Funding: This study was supported via funding from Prince Sattam bin Abdulaziz University, project number (PSAU/2023/R/1444).

Institutional Review Board Statement: Not applicable

Acknowledgments: This study was supported via funding from Prince Sattam bin Abdulaziz University, project number (PSAU/2023/R/1444).

Conflicts of Interest: The authors declare no conflict of interest.

References

- [1] D. Zhao, S. Yu, B. Sun, S. Gao, S. Guo, K. Zhao, Biomedical applications of chitosan and its derivative nanoparticles, *Polymers*. 10 (2018). <https://doi.org/10.3390/polym10040462>.
- [2] P. Baharlouei, A. Rahman, Chitin and Chitosan : Prospective Biomedical Applications in, *Marine Drugs*. 20 (2022) 460.
- [3] S. Bandara, H. Du, L. Carson, D. Bradford, R. Kommalapati, Agricultural and biomedical applications of chitosan-based nanomaterials, *Nanomaterials*. 10 (2020) 1–31. <https://doi.org/10.3390/nano10101903>.
- [4] A. Pellis, G.M. Guebitz, G.S. Nyanhongo, Chitosan: Sources, Processing and Modification Techniques, *Gels*. 8 (2022) 5–25. <https://doi.org/10.3390/gels8070393>.
- [5] S. Crognale, C. Russo, M. Petruccioli, A. D’annibale, Chitosan Production by Fungi: Current State of Knowledge, Future Opportunities and Constraints, *Fermentation*. 8 (2022). <https://doi.org/10.3390/fermentation8020076>.
- [6] M.A. Mohammed, J.T.M. Syeda, K.M. Wasan, E.K. Wasan, An overview of chitosan nanoparticles and its application in non-parenteral drug delivery, *Pharmaceutics*. 9 (2017). <https://doi.org/10.3390/pharmaceutics9040053>.
- [7] X. Gong, Y. Gao, J. Shu, C. Zhang, K. Zhao, Chitosan-Based Nanomaterial as Immune Adjuvant and Delivery Carrier for Vaccines, *Vaccines*. 10 (2022). <https://doi.org/10.3390/vaccines10111906>.
- [8] M.M. Ahmed, M.K. Anwer, F. Fatima, A.S. Alali, M.A. Kalam, A. Zafar, S. Alshehri, M.M. Ghoneim, Development of Apremilast Nanoemulsion-Loaded Chitosan Gels: In Vitro Evaluations and Anti-Inflammatory and Wound Healing Studies on a Rat Model, *Gels*. 8 (2022). <https://doi.org/10.3390/gels8050253>.
- [9] A. Zamboulis, S. Nanaki, G. Michailidou, I. Koumentakou, M. Lazaridou, N.M. Ainali, E. Xanthopoulou, D.N. Bikiaris, Chitosan and its derivatives for ocular delivery formulations: Recent advances and developments, *Polymers*. 12 (2020) 9–11. <https://doi.org/10.3390/polym12071519>.
- [10] S. Shim, H.S. Yoo, The Application of Mucoadhesive Chitosan Nanoparticles in Nasal Drug Delivery, *Marine Drugs*. 18 (2020) 1–17. <https://doi.org/10.3390/MD18120605>.
- [11] A.E. Caprifico, P.J.S. Foot, E. Polycarpou, G. Calabrese, Overcoming the blood-brain barrier: Functionalised chitosan nanocarriers, *Pharmaceutics*. 12 (2020) 1–20. <https://doi.org/10.3390/pharmaceutics12111013>.
- [12] M. Mohammed, M.S. Alnafisah, M.K. Anwer, F. Fatima, B.K. Almutairy, S.M. Alshahrani, A.S. Alshetaibi, A. Alalaiwe, M.H. Fayed, A.Z. Alanazi, M. Al Zahrani, M.M. Hailat, R. Al-Shdefat, Chitosan surface modified PLGA nanoparticles loaded with brigatinib for the treatment of non-small cell lung cancer, *Journal of Polymer Engineering*. (2019). <https://doi.org/10.1515/poly-eng-2019-0265>.

- [13] K.M. Noorulla, M. Yasir, F. Muzaffar, R. S, M.M. Ghoneim, A.S. Almurshedi, A.J. Tura, S. Alshehri, T. Gebissa, S. Mekit, M.M. Ahmed, A. Zafar, Intranasal delivery of chitosan decorated nanostructured lipid carriers of Buspirone for brain targeting: Formulation development, optimization and In-Vivo preclinical evaluation, *Journal of Drug Delivery Science and Technology*. 67 (2022) 102939. <https://doi.org/10.1016/j.jddst.2021.102939>.
- [14] M.K. Anwer, E.A. Ali, M. Iqbal, M.M. Ahmed, M.F. Aldawsari, A. Al Saqr, A. Alalaiwe, G.A. Soliman, Development of Chitosan-Coated PLGA-Based Nanoparticles for Improved Oral Olaparib Delivery: In Vitro Characterization, and In Vivo Pharmacokinetic Studies, *Processes*. 10 (2022). <https://doi.org/10.3390/pr10071329>.
- [15] B. Salehi, A. Venditti, M. Sharifi-Rad, D. Kręgiel, J. Sharifi-Rad, A. Durazzo, M. Lucarini, A. Santini, E.B. Souto, E. Novellino, H. Antolak, E. Azzini, W.N. Setzer, N. Martins, The therapeutic potential of Apigenin, *International Journal of Molecular Sciences*. 20 (2019). <https://doi.org/10.3390/ijms20061305>.
- [16] J.H. Yoon, M.Y. Kim, J.Y. Cho, Apigenin: A Therapeutic Agent for Treatment of Skin Inflammatory Diseases and Cancer, *International Journal of Molecular Sciences*. 24 (2023). <https://doi.org/10.3390/ijms24021498>.
- [17] R. Ranjan, K. Kishore, S. TJ, A.K. Jha, B.K. Ojha, S. Kumar, R. Kumar, Nutraceutical Potential of Vitexin: A Flavone Glycoside, *The Journal of Phytopharmacology*. 12 (2023) 44–50. <https://doi.org/10.31254/phyto.2023.12107>.
- [18] X. Yan, M. Qi, P. Li, Y. Zhan, H. Shao, Apigenin in cancer therapy: Anti-cancer effects and mechanisms of action, *Cell and Bioscience*. 7 (2017) 1–16. <https://doi.org/10.1186/s13578-017-0179-x>.
- [19] D. Wróbel-Biedrawa, K. Grabowska, A. Galanty, D. Sobolewska, I. Podolak, A Flavonoid on the Brain: Quercetin as a Potential Therapeutic Agent in Central Nervous System Disorders, *Life*. 12 (2022). <https://doi.org/10.3390/life12040591>.
- [20] F.J. Osonga, A. Akgul, R.M. Miller, G.B. Eshun, I. Yazgan, A. Akgul, O.A. Sadik, Antimicrobial activity of a new class of phosphorylated and modified flavonoids, *ACS Omega*. 4 (2019) 12865–12871. <https://doi.org/10.1021/acsomega.9b00077>.
- [21] Y. Xu, X. Li, H. Wang, Protective Roles of Apigenin Against Cardiometabolic Diseases: A Systematic Review, *Frontiers in Nutrition*. 9 (2022) 1–16. <https://doi.org/10.3389/fnut.2022.875826>.
- [22] A.N. Panche, A.D. Diwan, S.R. Chandra, Flavonoids: An overview, *Journal of Nutritional Science*. 5 (2016). <https://doi.org/10.1017/jns.2016.41>.
- [23] L.M.V.M. Ciumarnean, O. Runcan, S.C. Vesa, A.L. Rachis, V. Negrean, M.-G. Perné, V.I. Donca, T.-G. Alexescu, I. Para, G. Dogaru, The Effects of Flavonoids in Cardiovascular Diseases, *Molecules*. (18) (2020) 1–18. doi:10.3390/molecules25184320.
- [24] U.J. Jung, Y.Y. Cho, M.S. Choi, Apigenin ameliorates dyslipidemia, hepatic steatosis and insulin resistance by modulating metabolic and transcriptional profiles in the liver of high-fat diet-induced obese mice, *Nutrients*. 8 (2016). <https://doi.org/10.3390/nu8050305>.
- [25] Yousef A. Al-Turki, Semiconductor Packaging δ Connect to computer specimen Load cell, *Pharmaceutics*. 23 (2019) 839–843. <https://doi.org/10.1021/je400982r>.
- [26] F. Shakeel, S. Alshehri, M.A. Ibrahim, E.M. Elzayat, M.A. Altamimi, K. Mohsin, F.K. Alanazi, I.A. Alsarra, Solubility and thermodynamic parameters of apigenin in different neat solvents at different temperatures, *Journal of Molecular Liquids*. 234 (2017) 73–80. <https://doi.org/10.1016/j.molliq.2017.03.057>.
- [27] S. Parveen, S.K. Sahoo, Evaluation of cytotoxicity and mechanism of apoptosis of doxorubicin using folate-decorated chitosan nanoparticles for targeted delivery to retinoblastoma, *Cancer Nanotechnology*. 1 (2010) 47–62. <https://doi.org/10.1007/s12645-010-0006-0>.
- [28] M. Kazi, A. Alhajri, S.M. Alshehri, E.M. Elzayat, O.T. Al Meanazel, F. Shakeel, O. Noman, M.A. Altamimi, F.K. Alanazi, Enhancing oral bioavailability of apigenin using a bioactive self-nanoemulsifying drug delivery system (Bio-SNEDDS): In vitro, in vivo and stability evaluations, *Pharmaceutics*. 12 (2020) 1–22. <https://doi.org/10.3390/pharmaceutics12080749>.
- [29] I. Kazmi, F.A. Al-Abbasi, S.S. Imam, M. Afzal, M.S. Nadeem, H.N. Altayb, S. Alshehri, Formulation and Evaluation of Apigenin-Loaded Hybrid Nanoparticles, *Pharmaceutics*. 14 (2022). <https://doi.org/10.3390/pharmaceutics14040783>.
- [30] M. Muqtader A, F. Fatima, M. Khalid Anw, M. F. Aldawsa, G. A. Soliman, M. H. Fayed, Development and Characterization of Spray-dried Amorphous Solid Dispersion of Sildenafil: In vivo Evaluation, *International Journal of Pharmacology*. 16 (2020) 460–469. <https://doi.org/10.3923/ijp.2020.460.469>.
- [31] M. Muqtader Ahmed, F. Fatima, M. Abul Kalam, A. Alshamsan, G.A. Soliman, A.A. Shaikh, S.M. Alshahrani, M.F. Aldawsari, S. Bhatia, M. Khalid Anwer, Development of spray-dried amorphous solid dispersions of tadalafil using glycyrrhizin for enhanced dissolution and aphrodisiac activity in male rats, *Saudi Pharmaceutical Journal*. 28 (2020) 1817–1826. <https://doi.org/10.1016/j.jsps.2020.11.007>.
- [32] S.J. Gilani, M.N. Bin-Jumah, F.A. Al-Abbasi, M.S. Nadeem, S.S. Imam, S. Alshehri, M.M. Ahmed, M.M. Ghoneim, M. Afzal, S.I. Alzarea, N. Sayyed, I. Kazmi, Protective Effect of Fustin Against Ethanol-Activated Gastric Ulcer via Downregulation of Biochemical Parameters in Rats, *ACS Omega*. 7 (2022) 23245–23254. <https://doi.org/10.1021/acsomega.2c01341>.
- [33] P. Tran, Y.C. Pyo, D.H. Kim, S.E. Lee, J.K. Kim, J.S. Park, Overview of the manufacturing methods of solid dispersion technology for improving the solubility of poorly water-soluble drugs and application to anticancer drugs, *Pharmaceutics*. 11 (2019) 1–26. <https://doi.org/10.3390/pharmaceutics11030132>.
- [34] A. Vilatte, X. Spencer-Milnes, H.O. Jackson, S. Purton, B. Parker, Spray Drying Is a Viable Technology for the Preservation of Recombinant Proteins in Microalgae, *Microorganisms*. 11 (2023) 1–19. <https://doi.org/10.3390/microorganisms11020512>.
- [35] Y. Li, A.K.P. Mann, D. Zhang, Z. Yang, Processing impact on in vitro and in vivo performance of solid dispersions—a comparison between hot-melt extrusion and spray drying, *Pharmaceutics*. 13 (2021). <https://doi.org/10.3390/pharmaceutics13081307>.

- [36] M.F. Aldawsari, M.K. Anwer, M.M. Ahmed, F. Fatima, G.A. Soliman, S. Bhatia, A. Zafar, M.A. Aboudzadeh, Enhanced dissolution of sildenafil citrate using solid dispersion with hydrophilic polymers: Physicochemical characterization and in vivo sexual behavior studies in male rats, *Polymers*. 13 (2021) 1–15. <https://doi.org/10.3390/polym13203512>.
- [37] M.M. Ahmed, M.K. Anwer, G.A. Soliman, M.F. Aldawsari, A.A. Mohammed, S. Alshehri, M.M. Ghoneim, A.S. Alali, A. Alshetaili, A. Alalaiwe, S.I. Bukhari, A. Zafar, Application of hydrophilic polymers for the preparation of tadalafil solid dispersions: micromeritics properties, release and erectile dysfunction studies in male rats, *PeerJ*. 10 (2022). <https://doi.org/10.7717/peerj.13482>.
- [38] M.K. Anwer, M.M. Ahmed, M.F. Aldawsari, M. Iqbal, V. Kumar, Preparation and Evaluation of Diosmin-Loaded Diphenylcarbonate-Cross-Linked Cyclodextrin Nanosponges for Breast Cancer Therapy, *Pharmaceuticals*. 16 (2022) 19. <https://doi.org/10.3390/ph16010019>.
- [39] A.A. Alqahtani, M.M. Ahmed, A.A. Mohammed, J. Ahmad, 3D Printed Pharmaceutical Systems for Personalized Treatment in Metabolic Syndrome, (2023) 1–23.
- [40] T. Kassem, T. Sarkar, T. Nguyen, D. Saha, F. Ahsan, 3D Printing in Solid Dosage Forms and Organ-on-Chip Applications, *Biosensors*. 12 (2022). <https://doi.org/10.3390/bios12040186>.
- [41] B. Basa, G. Jakab, N. Kállai-Szabó, B. Borbás, V. Fülöp, E. Balogh, I. Antal, Evaluation of biodegradable PVA-based 3D printed carriers during dissolution, *Materials*. 14 (2021). <https://doi.org/10.3390/ma14061350>.
- [42] M.K. Anwer, M.M. Ahmed, M.F. Aldawsari, S. Alshahrani, F. Fatima, M.N. Ansari, N.U. Rehman, R.I. Al-Shdefat, Eluxadolone loaded solid lipid nanoparticles for improved colon targeting in rat model of ulcerative colitis, *Pharmaceuticals*. 13 (2020) 1–16. <https://doi.org/10.3390/ph13090255>.
- [43] L.E. Vallejo, J.M. Espitia, B. Caicedo, The influence of the fractal particle size distribution on the mobility of dry granular materials, *EPJ Web of Conferences*. 140 (2017) 4–7. <https://doi.org/10.1051/epjconf/201714003032>.
- [44] M.F. Aldawsari, M.M. Ahmed, F. Fatima, M.K. Anwer, P. Katakam, A. Khan, Development and characterization of calcium-alginate beads of apigenin: In vitro antitumor, antibacterial, and antioxidant activities, *Marine Drugs*. 19 (2021). <https://doi.org/10.3390/md19080467>.
- [45] A. Zafar, N.K. Alruwaili, S.S. Imam, O.A. Alsaidan, M.M. Ahmed, M. Yasir, M.H. Warsi, A. Alquraini, M.M. Ghoneim, S. Alshehri, Development and Optimization of Hybrid Polymeric Nanoparticles of Apigenin: Physicochemical Characterization, Antioxidant Activity and Cytotoxicity Evaluation, *Sensors*. 22 (2022) 1–19. <https://doi.org/10.3390/s22041364>.
- [46] S. Zhu, S. Khalafi, Z. Chen, J. Poveda, D. Peng, H. Lu, M. Soutto, J. Que, M. Garcia-Buitrago, A. Zaika, W. El-Rifai, Silencing of miR490–3p by *H. pylori* activates DARPP-32 and induces resistance to gefitinib, *Cancer Letters*. 491 (2020) 87–96. <https://doi.org/10.1016/j.canlet.2020.07.014>.
- [47] T. Školáková, M. Slámová, A. Školáková, A. Kadeřábková, J. Patera, P. Zámstný, Investigation of dissolution mechanism and release kinetics of poorly water-soluble tadalafil from amorphous solid dispersions prepared by various methods, *Pharmaceutics*. 11 (2019). <https://doi.org/10.3390/pharmaceutics11080383>.
- [48] C. Godugu, A.R. Patel, R. Doddapaneni, J. Somagoni, M. Singh, Approaches to improve the oral bioavailability and effects of novel anticancer drugs berberine and betulinic acid, *PLoS ONE*. 9 (2014). <https://doi.org/10.1371/journal.pone.0089919>.
- [49] A. Ribeiro, A. Figueiras, D. Santos, F. Veiga, Preparation and solid-state characterization of inclusion complexes formed between miconazole and methyl- β -cyclodextrin, *AAPS PharmSciTech*. 9 (2008) 1102–1109. <https://doi.org/10.1208/s12249-008-9143-8>.
- [50] D.R. Telange, A.T. Patil, A.M. Pethe, H. Fegade, S. Anand, V.S. Dave, Formulation and characterization of an apigenin-phospholipid phytosome (APLC) for improved solubility, in vivo bioavailability, and antioxidant potential, *European Journal of Pharmaceutical Sciences*. 108 (2017) 36–49. <https://doi.org/10.1016/j.ejps.2016.12.009>.
- [51] M.M. Ahmed, F. Fatima, M.K. Anwer, M.F. Aldawsari, Y.S.M. Alsaidan, S.A. Alfaiz, A. Haque, A. AZ, K. Alhazzani, Development and characterization of Brigatinib loaded solid lipid nanoparticles: In-vitro cytotoxicity against human carcinoma A549 lung cell lines, *Chemistry and Physics of Lipids*. 233 (2020) 105003. <https://doi.org/10.1016/j.chemphyslip.2020.105003>.
- [52] K. Anwer, E.A. Ali, M. Iqbal, M.M. Ahmed, M.F. Aldawsari, A. Al Saqr, M.N. Ansari, M.A. Aboudzadeh, Development of Sustained Release Brigatinib Loaded Lipid-Polymer Hybrid Nanoparticles with Improved Oral Bioavailability, (2022).
- [53] E. H. Moglad, F. Fatima, M. Muqtader A, V. Devanathad, M. Khalid Anw, M. F. Aldawsa, Development of Topical Antibacterial Gel Loaded with Cefadroxil Solid Lipid Nanoparticles: In vivo Wound Healing Activity and Epithelialization Study, *International Journal of Pharmacology*. 16 (2020) 298–309. <https://doi.org/10.3923/ijp.2020.298.309>.
- [54] F. Fatima, M.F. Aldawsari, M.M. Ahmed, M.K. Anwer, M. Naz, M.J. Ansari, A.M. Hamad, A. Zafar, M. Jafar, Green synthesized silver nanoparticles using *tridax procumbens* for topical application: Excision wound model and histopathological studies, *Pharmaceutics*. 13 (2021). <https://doi.org/10.3390/pharmaceutics13111754>.
- [55] M.M. Ahmed, F. Fatima, A.B. Mohammed, Olive Oil Based Organogels for Effective Topical Delivery of Fluconazole : In-vitro Antifungal Study, 32 (2020) 29–36. <https://doi.org/10.9734/JPRI/2020/v32i2530821>.
- [56] M.K. Anwer, M.M. Ahmed, A. Alshetaili, B.K. Almutairy, A. Alalaiwe, F. Fatima, M.N. Ansari, M. Iqbal, Preparation of spray dried amorphous solid dispersion of diosmin in soluplus with improved hepato-renal protective activity: In vitro anti-oxidant and in-vivo safety studies, *Journal of Drug Delivery Science and Technology*. 60 (2020) 102101. <https://doi.org/10.1016/j.jddst.2020.102101>.
- [57] M. Mohammed, M.S. Alnafisah, M.K. Anwer, F. Fatima, B.K. Almutairy, S.M. Alshahrani, A.S. Alshetaili, A. Alalaiwe, M.H. Fayed, A.Z. Alanazi, M. Al Zahrani, M.M. Hailat, R. Al-Shdefat, Chitosan surface modified PLGA nanoparticles loaded with

- brigatinib for the treatment of non-small cell lung cancer, *Journal of Polymer Engineering*. 39 (2019) 909–916. <https://doi.org/10.1515/polyeng-2019-0265>.
- [58] M.M. Ahmed, M.K. Anwer, F. Fatima, M.F. Aldawsari, A. Alalaiwe, A.S. Alali, A.I. Alharthi, M.A. Kalam, Boosting the Anti-cancer Activity of Sunitinib Malate in Breast Cancer through Lipid Polymer Hybrid Nanoparticles Approach, *Polymers*. 14 (2022). <https://doi.org/10.3390/polym14122459>.
- [59] M.A. Azad, D. Olawuni, G. Kimbell, A.Z.M. Badruddoza, M.S. Hossain, T. Sultana, *Polymers for extrusion-based 3D printing of pharmaceuticals: A holistic materials–process perspective*, 2020. <https://doi.org/10.3390/pharmaceutics12020124>.
- [60] M.P. Schwicker, N.D. Nikolov, M. Häßel, Strength Optimization and Strength Prediction of Fused Deposition Modelled Specimens Based on Process Parameters, *International Journal of Mechanical Engineering and Robotics Research*. 11 (2022) 527–534. <https://doi.org/10.18178/ijmerr.11.7.527-534>.
- [61] M.M. Ahmed, F. Fatima, A. Alnami, M. Alsenaidy, Design and Characterization of Baricitinib Incorporated PLA 3D Printed Pills by Fused Deposition Modeling : An Oral Pill for Treating Alopecia Areata, (2023).
- [62] M.M. Ahmed, M.K. Anwer, F. Fatima, M. Iqbal, E. Ezzeldin, A. Alalaiwe, M.F. Aldawsari, Development of ethylcellulose based nanosponges of apremilast: In vitro and in vivo pharmacokinetic evaluation, *Latin American Journal of Pharmacy*. 39 (2020) 1292–1299.
- [63] R. Al-Shdefat, B.E. Ali, M.K. Anwer, M.H. Fayed, A. Alalaiwe, G.A. Soliman, Sildenafil citrate-Glycyrrhizin/Eudragit binary spray dried microparticles: A sexual behavior studies on male rats, *Journal of Drug Delivery Science and Technology*. 36 (2016) 141–149. <https://doi.org/10.1016/j.jddst.2016.10.004>.